

Electron Microscopy of Irradiation Effects in Space

Radiation-damaged lunar and meteoritic grains tell us about solar system history and synthesis of molecules in space.

M. Maurette and P. B. Price

The study of radiation damage effects in minerals and the use of these effects in diverse fields of science grew out of the discovery of fossil fission fragment tracks in a uranium-bearing mica (1). However, although that discovery was made with a transmission electron microscope, virtually all of the subsequent studies reported in more than 1500 papers between 1963 and 1970 were based on the observation of etched tracks with the optical microscope, which was easy and convenient to use. The successful return of lunar samples, with their high concentrations of radiation damage features, opened up a new area of research in which transmission electron microscopy (TEM) has played a dominant role. With neither an atmosphere nor a large-scale magnetic field to stop or deflect the solar wind and low-energy nuclear particles in space, the moon has an intensely irradiated surface. The smallest lunar dust grains, for example, are loaded with radiation damage features that tell a fascinating story, but one that can be deciphered only with high-resolution TEM techniques. In this article we describe several discoveries that we and our colleagues have made in studies of lunar material and show how our results lead to inferences about other extraterrestrial features, such as the parent bodies of meteorites, the early solar nebula, and the interstellar medium.

Solar Wind Implantation Effects

The solar wind is the expanding solar corona, which propagates at an average speed corresponding to an ion energy of 1 kiloelectron volt per atomic mass unit (amu). Measurements of the relative abundances of the elements H, He, O, Ne, Si, Ar, and Fe indicate that its average composition is similar to that of the solar corona (2). Intense radiation damage effects are produced in the surface regions of lunar dust grains by solar wind ions, which have a projected range of a few hundred angstroms in solids. Even grains buried at great depths in the lunar soil or deep inside lunar fragmental rocks have damaged "skins," showing that they were at one time exposed at the surface of the lunar soil. It is possible, by high-voltage (~ 1 Mev) electron microscopy (HVEM), to study solar wind effects at different epochs in the past by analyzing grains extracted either from different depths in one of the lunar core tubes or from breccias compacted at very different times in the distant past.

Solar wind radiation damage parameters and their aging characteristics. An artificial solar wind irradiation can be simulated by crushing single crystals of various minerals into micrometer-sized grains and irradiating them with high doses ($\approx 10^{15}$ per square centimeter) of

low-energy ions (between 0.2 and 6 keV/amu) ranging from hydrogen up to lead nuclei. Above a critical dose that depends on both the mineral and the projectile, the grains become severely rounded by ion sputtering and become coated to a minor extent with redeposited sputtered material and to a major extent with an ultrathin, amorphous layer of radiation-damaged material (Fig. 1, a and b) that results from the overlap of the very short (~ 100 Å) tracks of the ions (3). Helium ions are about 100 times as effective as protons and one-tenth as effective as argon ions; when weighted by their relative abundance in the solar wind they should be the dominant rounding and coating ions in the solar cavity (the region of the solar system swept out by the solar wind) (4).

With HVEM, lunar dust grains are observed to have old coatings, which are similar in appearance to the fresh coatings produced in the calibration experiments (Fig. 1c) but result from ancient implantation of solar wind nuclei into the grains (3, 5, 6). To characterize each lunar soil sample we measure Δ , the thickness of the amorphous coating; $\delta(\Delta)$, the distribution of coating thicknesses; and $P(\Delta)$, the proportion of grains with a coating. Both old and fresh coatings are stable when viewed in the HVEM beam and unchanged by a low-temperature thermal annealing. During annealing at a high temperature ($\sim 800^\circ\text{C}$ for feldspar) the coatings disappear, being transformed into tiny crystallites that are visible by HVEM (3, 7).

Energy of the ancient solar wind. Experimentally the thickness of the amorphous coating produced by He ions varies as $\sim E^{0.5}$ for energies (E) between 0.2 and 3 keV/amu (4, 8). From our measurements of sputtering by He ions (discussed below) we infer that on lunar feldspar grains the solar wind builds up an equilibrium coating thickness in ~ 2000 years and that thereafter

Dr. Maurette is with Laboratoire Rene Bernas, 91406 Orsay and Institut d'Optique Electronique du CNRS, 31 Toulouse, France; Dr. Price is with the Department of Physics, University of California, Berkeley 94720.

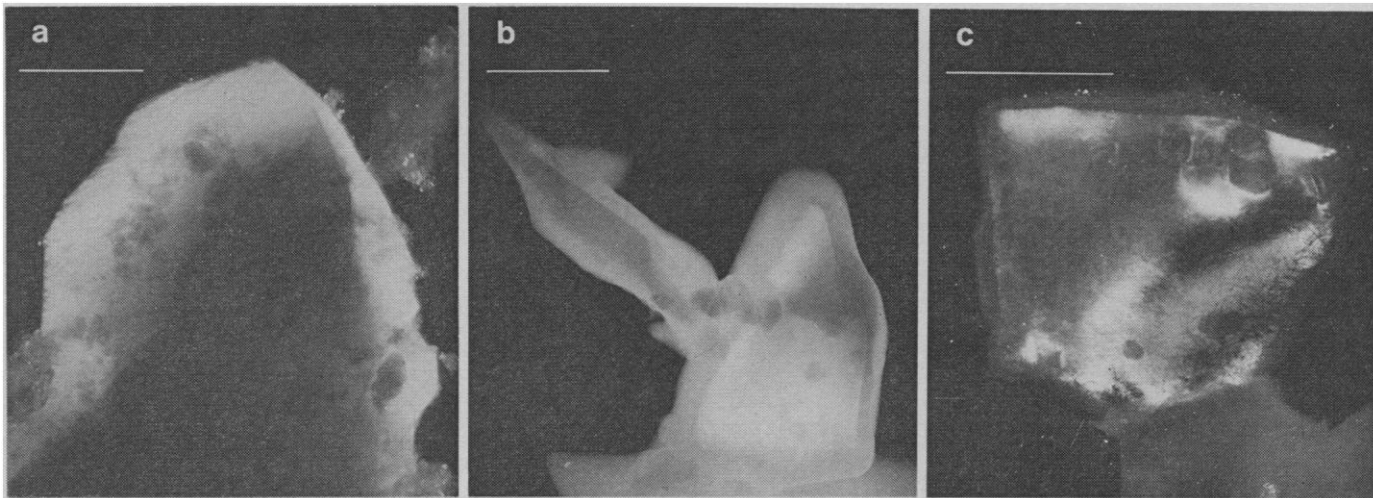


Fig. 1. Dark-field 1-Mev electron micrographs of micrometer-sized feldspar grains (a) irradiated with He ions with energies of 0.2 keV/amu, (b) irradiated with He ions with energies of 6.5 keV/amu, and (c) extracted from the lunar soil. Scale bars = 1 μm . The He ion flux, 10^{17} cm^{-2} , was chosen to simulate a 2000-year exposure in the solar wind. The initially angular grains in (a) and (b) have been rounded as a result of ion sputtering, and amorphous coatings of radiation-damaged material, whose thickness increases with ion energy, can be observed as dark linings around the grains. The lunar grain is also rounded, has a coating of thickness intermediate between that in (a) and (b), and also contains a high density of tracks. [Courtesy of Institut d'Optique Electronique, Toulouse]

the coating propagates with a constant thickness into the shrinking grain as sputtering removes the outer atoms. In a well-stirred lunar soil the coating thicknesses provide 2000-year snapshots of solar wind energies over the lifetime of the soil, typically $\sim 3.5 \times 10^9$ years.

Figure 2 shows $\delta(\Delta)$ measured on ≈ 500 individual grains extracted at random from the 3-meter core tube obtained on the Apollo 15 mission (9). When we convert from Δ to E by means of the calibration experiments, such histograms give the frequency distribution of 2000-year periods during which the solar wind has an "average" energy E (8, 10). The most probable energy in the ancient solar wind is ~ 1 keV/amu, the same as the average energy in the contemporary solar wind. There is a rather high frequency of periods of low solar wind energy at the moon. The lowest energy so far detected (~ 0.2 keV/amu) happens to correspond to the minimum energy required for solar wind nuclei to escape contemporary magnetic fields at the sun (11). It could thus be argued that magnetic field activity at the sun has not been lower than its present value. There is an approximately exponential decrease in the frequency of 2000-year periods of high solar wind energy at the moon, with the highest energy, ~ 5 keV/amu, being outside the limits of the last few years. Note that there is no indication of any change in the mean solar wind energy over geologic time.

Solar wind sputtering erosion rate.

Estimates of the sputtering erosion rate of the solar wind impinging on the lunar surface range from ~ 0.5 (12) to 0.04 \AA/year (13). The former value may be too high because it was obtained from an experiment in which the beam current may have been high enough to heat the target, and atoms may not have had time to reach more tightly bound positions by surface diffusion between the sputtering events that removed their neighbors. The latter value was derived for an initially smooth, flat surface and probably underestimates the rate for an actual dust grain surface, a portion of which is constantly exposed at a shallow angle to the solar wind beam and is thus eroded at a much higher rate than a surface normal to the beam.

With the HVEM it is possible to simulate the actual lunar geometry by directly measuring the sputtering erosion rate of micrometer-sized angular grains of various minerals. A double irradiation technique is used (4, 14). A thick amorphous coating ($\Delta \approx 800 \text{ \AA}$) produced with higher-energy ions (3 keV/amu) is gradually eroded away with lower-energy ions (0.2 keV/amu) that leave a thin residual coating ($\Delta \approx 150 \text{ \AA}$) on the grains. The results show that the solar wind erosion rate will greatly depend on the mineral type, being 20 times higher for glassy grains than for ilmenite (FeTiO_3) grains. Furthermore, the absolute value obtained for the common lunar mineral feldspar, 0.5 \AA/year for a surface con-

tinuously exposed, agrees well with the estimate of Wehner *et al.* (12) and is much higher than currently accepted values.

One implication of these results is that the mineralogical composition of the smallest grains in a sample of mature or well-worked soil should be different from that of the larger grains and should reach a saturation composition determined by equilibrium between the generation of small grains and their loss by erosion (10). Observations of mature soil samples by HVEM (6) do indeed show that in grains smaller than $5 \mu\text{m}$ the proportion of glass is generally much lower (~ 10 percent) than in the coarse grains (~ 50 percent) and is not correlated with the various maturity indexes that we will discuss later. Another implication is that the flux of picogram particles in space, inferred from counts of submicrometer craters on the surfaces of lunar rocks and soil grains (15), may be underestimated as a result of sputtering loss of the smallest craters. For example, the lifetime of a crater $1 \mu\text{m}$ deep would be only 2×10^4 years on a surface eroding at 0.5 \AA/year .

Peculiar physicochemical properties of amorphous coatings. The coatings can be thought of as a dense jungle of completely overlapping nuclear particle tracks covering the surfaces of grains. In such a peculiar, heavily radiation-damaged material the implanted solar wind species should diffuse and react chemically much faster than in ordinary crystalline matter. Furthermore, the

high concentration of stored energy in the coatings could possibly be released during grain collisions, heat metamorphism, and so forth. Let us consider three of the implications of these reactive coatings.

1) They serve as a sticking agent. The micrometer-sized lunar dust grains extracted from mature soil samples are observed by HVEM to be welded aggregates of even smaller particles (4, 6, 16). No other type of "glue" than the amorphous coatings is present at the grain boundaries. Thermal sintering studies (4, 17) show that grains with either a natural or a simulated solar wind coating can form pellets of sintered dust at low temperatures ($\approx 600^\circ\text{C}$) whereas fresh grains cannot be sintered below $\sim 1100^\circ\text{C}$. Thus the amorphous coatings are probably responsible for the formation of the microscopic soil breccias on the moon, and the release of stored energy may be the active sticking ingredient, as A. Turkevich has suggested.

2) Outgassed species can be reimplanted into lunar soil. Atoms and molecules in the tenuous lunar atmosphere can, through interaction with the solar wind, be driven into the surfaces of soil grains at much shallower depths than those reached by the solar wind itself. An example of a lunar atmospheric species is ^{40}Ar from the radioactive decay of ^{40}K in lunar rocks (18). Once within an amorphous coating, these reimplanted species should diffuse rapidly and become indistinguishable from the solar wind species, which were implanted at much higher energy. It is thus not possible, by mass spectrometric analysis of products released in stepwise heating experiments, to distinguish the origins of species implanted at different energies into amorphous coatings (19).

3) Small molecules are synthesized in amorphous coatings. In the laboratory, implantation of low-energy ions of H, C, and N into silicate targets with amorphous coatings gives a highly specific mixture of small molecules (19, 20): carbon compounds containing no more than three carbon atoms, a relatively high abundance of OH and CNH species, and a very low abundance of nitrogen oxides ($\text{NO}/\text{CNH} \approx 10^{-3}$). In contrast, other processes proposed to explain the abiotic synthesis of molecules in space are somewhat extreme, either leading to rich mixtures of carbon compounds containing such molecules as C_{18} (21) or hardly synthesizing any-

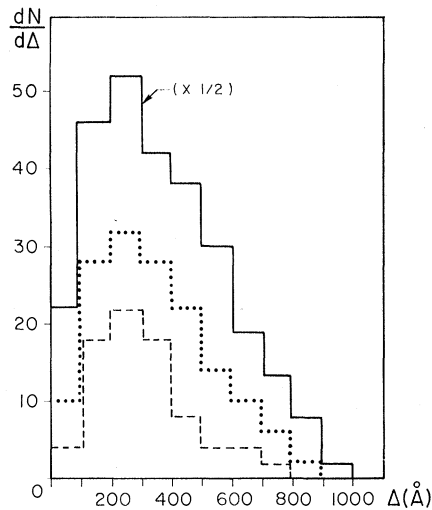


Fig. 2. Distribution of coating thicknesses for grains extracted from the Apollo 15 deep drill core tube. The solid line is the overall distribution in a mixture of grains from many levels in the core. The dotted and dashed lines give the distributions at depths of ~ 20 cm and ~ 250 cm, respectively. [Courtesy of J. Borg]

thing but H_2 (22). The process we call ion implantation synthesis, which takes place within amorphous coatings, satisfactorily explains the formation of carbon compounds in the crystalline component of the lunar soil (23) and may well play a role in the synthesis of interstellar molecules, such as OH, that are difficult to explain by other processes (4).

Maturity indexes and the macroscopic properties of the lunar regolith. Through

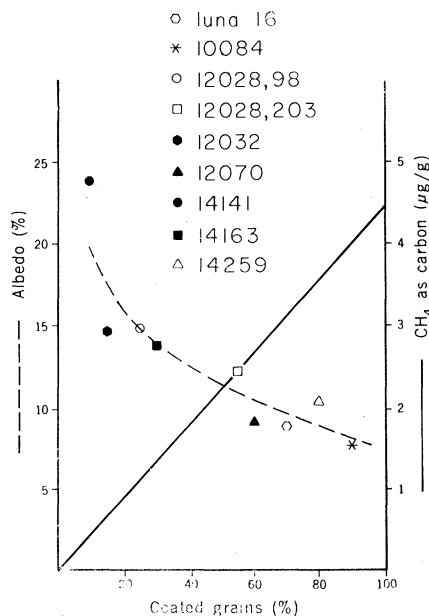


Fig. 3. Correlations between albedo, the proportion of coated grains, and the carbon concentration in the same soil sample.

complex interactions with the solar wind, higher-energy nuclei, and impacting objects of all sizes, the lunar regolith (or surface soil and rocks) matures. During maturation solar wind implantation leads to synthesis of carbon compounds, the concentration of glassy agglutinates increases, surfaces develop microcraters, the albedo of the lunar soil is modified, and so forth.

The proportion of grains with an amorphous coating, $P(\Delta)$, is a good index of maturity. Figure 3 shows the correlations between $P(\Delta)$, the concentration of total carbon (24), and the albedo for the same lunar soil samples (25). That total carbon should be directly correlated with $P(\Delta)$ is now well understood, since solar wind ion implantation synthesis has to occur in the amorphous coatings and the species produced thereby are not severely redistributed during the maturation of the crystalline component. On the other hand, the correlation between $P(\Delta)$ and lunar albedo may or may not be direct. The first hypothesis, verified by measuring the albedo of an Apollo 11 soil sample as a function of grain size (14), was that the small grains cover the surfaces of the large ones and thus are responsible for the optical properties of a mature soil sample. Another hypothesis was that the low albedo of soils with high $P(\Delta)$ values is a result of the peculiar dielectric structure of the small grains, whose amorphous coatings would have a lower refractive index than that of the underlying crystals (3). But, in addition, soil samples with a high $P(\Delta)$ contain a high proportion of microaggregates in which the constituent dust particles might have a peculiar mineralogical composition. The albedo function may thus depend on several factors.

Solar wind gas bubbles. Solar wind gas atoms may diffuse from an amorphous coating deeper into a lunar soil grain and coagulate into tiny bubbles, less than 100 Å in diameter (26, 27), which can be seen in grains where the track density is low enough not to obscure them. In lunar soil grains the density of bubbles can be as high as 10^{15} cm^{-3} and correlates with the solar wind gas concentration (27).

Composition of very heavy nuclei in the contemporary solar wind. Mica, because of its extraordinarily anisotropic etching, is capable of recording etchable pits at the points of impact of individual heavy solar wind nuclei (28). The etch pits, which are very shallow,

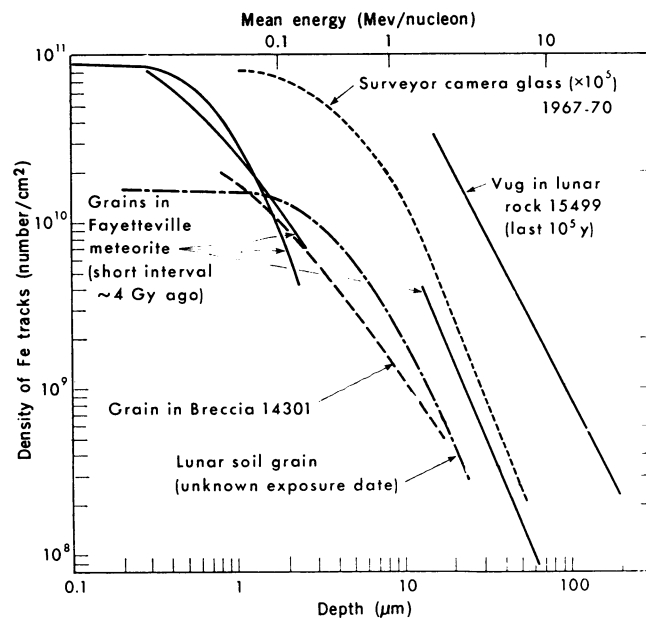
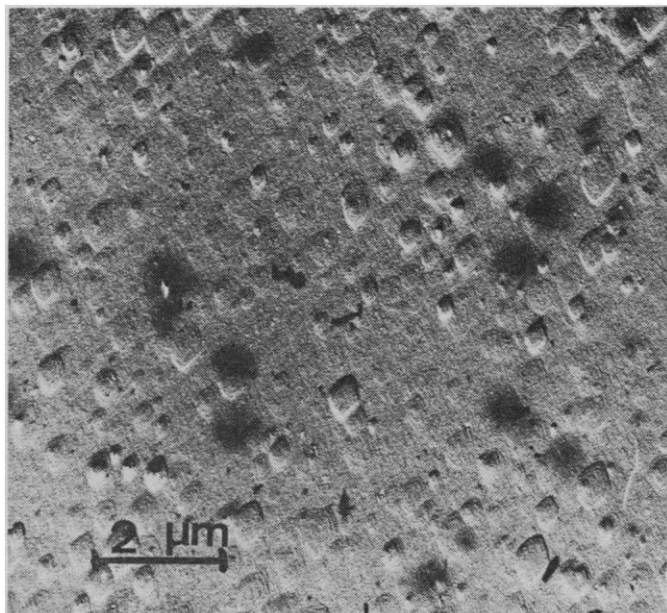


Fig. 4 (left). Electron micrograph (100 kev) of a replica of a mica surface that was irradiated with lead nuclei (1 kev/amu), then etched for 1 hour in a dilute HF solution. Each shallow pit corresponds to the very short, etched track of a lead ion. [Courtesy of J. Borg and E. Zinner] Fig. 5 (right). Steep track density gradients by TEM on replicas of etched grains from soils, a lunar breccia, a gas-rich meteorite, and a cavity on the surface of a lunar rock, compared with the track density gradient in the Surveyor camera glass.

can be studied by observing surface replicas in the electron microscope (Fig. 4). After a particular etch time, the pit diameter is an increasing function of atomic number and the depth increases with ion velocity. By comparing pits in mica exposed to various ions in an accelerator with pits in a piece of mica exposed to the solar wind during the Apollo 17 mission, it has been shown that the Fe/H ratio in the solar wind during that mission was similar to that in the corona and that ions with atomic number $Z \geq 60$ were no more than about twice as abundant in the solar wind as in the corona (29). It should be noted, however, that the solar wind composition does vary with time and that the composition during the brief period of Apollo 17 may not be representative of the long-term average composition.

Heavily damaging ions ($Z \geq 20$) with energies greater than that of the solar wind produce tracks in insulating solids. From ~ 5 to ~ 100 kev/amu their range is so small ($< 2 \mu\text{m}$) that the tracks can be seen only by electron microscopy. At higher energies individual tracks are long enough to be made visible in an optical microscope by chemical etching, but often the density of such tracks in an unshielded extra-terrestrial sample is so high that the sample would disintegrate if etched for the normal time. Instead, it is necessary to utilize the high resolution of the

electron microscope to look at either latent tracks or very lightly etched tracks. A good rule of thumb is that electron microscopy is essential whenever the product of particle flux and exposure time is such that the track density exceeds 10^8 cm^{-2} .

Track "aging" processes. The structure of a latent track can be altered both by thermal annealing and by a high background of ionizing radiation. In the first study of fission fragment tracks in mica (30) their fading in the highly ionizing beam of a 100-kev electron microscope made a detailed study impossible. Even in the beam of a 1.5-Mev electron microscope, with its 15 times lower ionization rate, Kr ion tracks rapidly disappeared in feldspar and pyroxene crystals (7). In contrast, "old" tracks in lunar dust grains with an amorphous coating are stable when viewed by HVEM. We think that the amorphous coating of heavily radiation-damaged matter acts as a reservoir of defects that, during the hottest part of the lunar thermal cycle, can diffuse along the cores of the latent tracks to form clusters of defects more stable than individual defects. Recent electron microscope experiments have demonstrated that the portions of tracks near a high concentration of radiation damage can be stabilized (7).

The stabilization of tracks by solar wind radiation damage may explain the apparent disagreement between our two

groups in their search for high densities of latent tracks in gas-rich meteorites, so named because of the high concentration of solar wind gases implanted in the constituent grains before compaction. In crushed fragments extracted from the fine-grained matrices of Weston, Kapoeta, and Pesyanoe meteorites no latent tracks were ever found (31, 32), whereas high densities of latent tracks are commonly found (26, 33) in ultrathin sections of Fayetteville and Pesyanoe ion-thinned with very high doses of 5-kev Ar ions, which are known to produce thin amorphous coatings on the grains.

Down to several centimeters in lunar soil, and much deeper in solid lunar rock, the maximum temperature is high enough to cause detectable changes in track structure. Studies with heavy ion beams at the Berkeley Hilac (34) and the Manchester cyclotron (7, 35) have shown that the lightly damaged portion of a fresh track begins to fade at a relatively low temperature, leaving an aged track consisting of the more resistant, heavily damaged portion. If, for example, we bombard feldspar with Fe ions of energies up to 10 Mev/amu, we find a broad distribution of etched track lengths including a small fraction that etch over the entire range of an Fe ion of 10 Mev/amu, whereas natural tracks of Fe ions in most lunar feldspars have a rather narrow distribution of etched lengths corresponding to an energy in-

terval of only about 3 or 4 Mev/amu. We find that the high-energy parts of fresh tracks in feldspar begin to age in a few days at the maximum lunar surface temperature ($\sim 130^\circ\text{C}$). Small-angle x-ray scattering measurements on irradiated mica (36) show how the track structure changes by thermal annealing. Small clusters of defects formed along the paths of the incident ions coagulate into larger, more widely separated clusters that reach a maximum size of about 20 Å as the annealing temperature is raised to 300°C , but then shrink in size and eventually disappear with increasing temperature.

Track aging is useful as an indicator of various dynamic processes in the regolith, but it may hamper efforts to infer characteristics of nuclear particles in space from measurements of track parameters. For example, in order to infer the VVH/VH abundance ratio [where VVH (very very heavy) means $Z \approx 30$ and VH (very heavy) means $20 < Z < 30$] in ancient solar and galactic cosmic rays from track length distributions, we must learn how to correct for the decrease of track etching rate with aging. Fortunately, most TEM applications concern either relatively fresh tracks registered in detectors exposed to contemporary radiation or gradients in the density of ancient tracks, which are not noticeably altered by aging (37).

Ancient Solar Particles

The first HVEM observations of tracks in lunar dust grains led to the discovery of intense fluxes of heavy ions with energies intermediate between those of the solar wind nuclei and those of the more energetic solar flare particles (6, 31, 33, 38, 39). For convenience, and without wishing to imply an origin, we refer to ions with $5 < E \lesssim 500$ keV/amu as suprathreshold ions. The track densities fall off steeply in the first 1 to 2 μm of depth in soil grains. Either a partial dust covering or a gradual removal of surface by some erosional process will lower the observed track gradient (40), giving only a lower limit for the steepness of the energy spectrum of suprathreshold ions. We have used two different approaches in studying track gradients of suprathreshold ions. In both cases replicas of lightly etched, polished sections were studied by TEM. At Berkeley (41, 42) only grains with extremely steep track gradients were analyzed (see Fig. 5). Starting at the outer surface

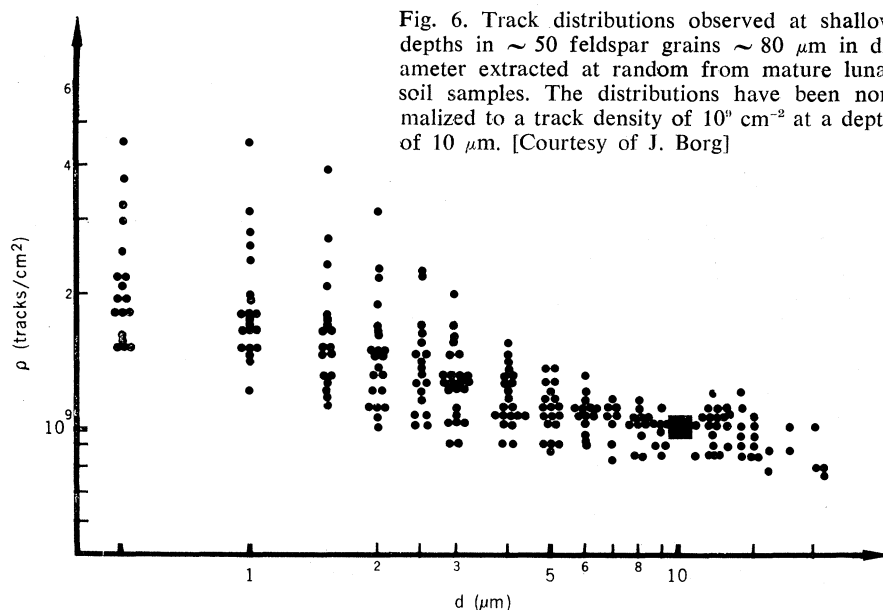


Fig. 6. Track distributions observed at shallow depths in ~ 50 feldspar grains $\sim 80 \mu\text{m}$ in diameter extracted at random from mature lunar soil samples. The distributions have been normalized to a track density of 10^{11} cm^{-2} at a depth of $10 \mu\text{m}$. [Courtesy of J. Borg]

with a track density limited by TEM resolution to no more than $\sim 10^{11} \text{ cm}^{-2}$, the density at a depth of $50 \mu\text{m}$ has dropped to as low as 10^8 cm^{-2} . In a typical soil sample grains with such steep gradients are rare, having been exposed for a short time, usually in only one orientation, on the very surface of the regolith. At Orsay, Borg (43) chose at random about 500 feldspar grains $\sim 80 \mu\text{m}$ in diameter from a mature soil sample. As one would expect, most (~ 95 percent) of the grains had much shallower track gradients and a higher track density at their center (often $> 5 \times 10^9 \text{ cm}^{-2}$) than those shown in Fig. 5. Both features would be expected for grains that have been exposed over a long time, at various depths, and in various orientations in a mature soil sample. A small fraction of the random sample of $80\text{-}\mu\text{m}$ grains (5 to ~ 50 percent depending on the soil) has a steep gradient in the outer 2 to $\sim 5 \mu\text{m}$ superimposed on the shallow gradient (Fig. 6), which indicates that in a mature soil with a complex history of many exposures some grains reside at the surface long enough to acquire a detectable suprathreshold track gradient. Borg also found that the proportion of such grains in various soils appears not to be correlated with either $P(\Delta)$ or the proportion of grains having $\Delta > 800 \text{ \AA}$. Thus the suprathreshold ions are probably not emitted in correlation with the solar wind.

Comparative studies have been made (41, 42) of solar flare track gradients at depths down to $\sim 10^3 \mu\text{m}$ in grains within gas-rich meteorites, lunar breccias, and the lunar soil and also in

crystals at the surfaces of rocks protected from normal erosion (44–46). These grains have sampled solar flares emitted in different epochs ranging from the last $\sim 10^3$ years to the early beginnings of the solar system. A comparison of the gradients, some of which are shown in Fig. 5, with gradients in recent flares (discussed below) shows that the average energy distribution in solar flares has not changed significantly over the last several billion years (44, 45).

The earliest preserved track gradients are in grains within gas-rich meteorites. Papanastassiou *et al.* (47) have measured an age of 3.7×10^9 years for an igneous chip inside the Kapoeta gas-rich meteorite. It is not yet known whether some other gas-rich meteorites were assembled even closer in time to the beginning of the solar system, but track studies in such objects would be very exciting, for it is likely that the sun's angular momentum, surface magnetic field, and solar flare rate were decreasing during its early phase. The most likely prospects are the carbonaceous chondrites, some of which have recently been found (48) to contain track-rich olivine grains with track gradients similar to those in Fig. 5. Further track studies in these meteorites, which are generally believed to be the most primitive objects in the solar system, may make it possible to date their time of compaction (48).

Combining observations of both suprathreshold gradients and solar flare gradients, we find that the average flux of Fe-group ions in space continues to rise with decreasing energy down to energies as low as 5 or 10 keV/amu, as

shown in Fig. 7. Present techniques do not permit us to deal with individual tracks at lower energies. The energy spectra in Fig. 7 were determined from favorable samples subjected to little erosion. Even so, we have indicated by arrows where the curve, because of possible erosion, should be regarded only as a lower limit to the true spectrum.

Contemporary Solar Particles

At about the time when ancient suprathermal and solar flare tracks were first seen by HVEM, Fe tracks from recent solar flares were found in a flint glass filter from the Surveyor 3 television camera, which was exposed on the moon during the period of maximum solar activity in 1967 to 1969 (49, 50). An unexpected and important consequence of this work was the discovery (50) that heavy elements such as Fe are emitted in far higher than solar proportions in solar flares (a factor of about 100), the degree of enrichment being a decreasing function of energy and an increasing function of atomic number. There is still no good explanation for the phenomenon, but it is important for the lunar scientist to remember that he would drastically underestimate the densities of heavy ion tracks if he assumed solar abundances and used proton or alpha-particle fluxes measured on satellites during flares.

During the Apollo 16 mission a small solar flare produced heavy ion tracks in mica, glass, and Lexan detectors that were exposed outside the lunar module and later thoroughly studied by electron and optical microscopy (51). In this flare the flux monotonically increased with decreasing energy down to as low as 10 keV/amu. However, the total energy output in this flare was negligible compared with that in flares such as the great ones of August 1972, and we cannot be sure that the energy spectra in large flares extend down to low enough energies to account for the ancient suprathermal ion tracks.

Several times a year large fluxes of suprathermal protons (5 to ~50 keV) coming predominantly from the direction of the sun have been detected in interplanetary space (52), and over about half of each lunar month protons of ~30 to 100 keV, probably accelerated by interaction of the solar wind with the earth's magnetosphere, are detected by a satellite in lunar orbit (53). To detect heavy ions of such low energy would be difficult with existing elec-

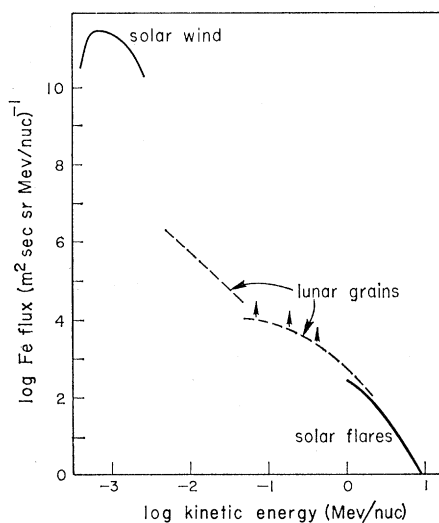


Fig. 7. Average flux of suprathermal Fe ions in interplanetary space based on steep track gradients in lunar grains (see Fig. 5). The flux is intermediate between that of the solar wind and that definitely known to come from solar flares.

tronic detectors on satellites, and it remains a mystery whether the suprathermal heavy ions that produce tracks in lunar and meteoritic grains originated in the solar wind, in solar flares, or in some other process such as shock wave acceleration of ions in interplanetary space.

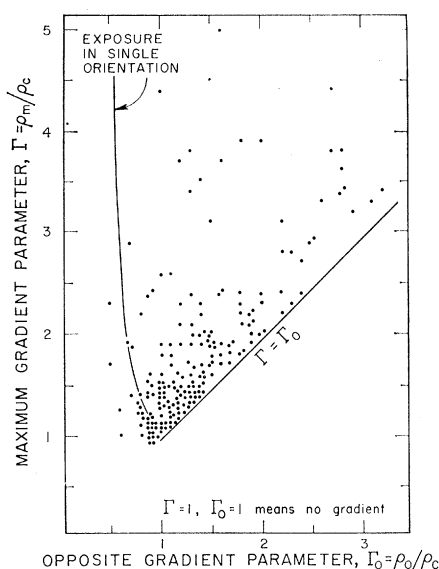


Fig. 8. Statistical analysis of solar flare track gradients in feldspar grains ~80 μm in diameter from various lunar soil samples. In each grain the track densities are measured at the center (ρ_c), ~3 μm in from the edge with the highest track density (ρ_m), and ~3 μm in from the opposite edge (ρ_o). The maximum gradient parameter, $\Gamma = \rho_m/\rho_c$, and the opposite gradient parameter, $\Gamma_o = \rho_o/\rho_c$, are plotted. The curves are part of the soil history computer program of G. Comstock. [Courtesy of J. Borg and G. Comstock]

Regolith Histories in the Solar System

The surfaces of planets and moons that are not shielded by an atmosphere or a magnetosphere evolve as a result of bombardment by charged particles and meteorites. If the gravitational field is strong enough to retain the debris, meteoritic impacts transform an initially rocky surface into a "regolith" (54), which in the case of the moon consists of a mixture of igneous rock fragments, dust grains, glassy agglutinates, and rocks called breccias that result from the compaction of fragments of soil and rocks. The position and orientation of a dust grain at an initial depth d in the regolith change with time: a nearby impact may bury the grain with an ejecta blanket of thickness δ ; a direct impact may excavate the grain if the overlying crater has a depth $D > d$, or the grain may be incorporated into a breccia and perhaps released by some subsequent impact. Such processes may result in shock or thermal metamorphism.

The track distributions measured by electron microscopy in soil or breccia grains from the surface and from various depths in drill cores help to determine the time constants for "gardening" to various depths in the regolith. Figure 8 shows one type of statistical analysis based on gradients of track density around the edges of lunar soil grains. Comstock and Langevin recently developed a Monte Carlo computer code that generates a theoretical dust grain at a depth d and follows its history of excavations and burials (16). They vary d , D , and δ , as well as the time intervals between cratering and layering, the steady state rate of burial, and the frequency of exposure of a grain at the top surface of the regolith, in order to get a best fit to the experimental characteristics of track distributions such as those in Fig. 8.

The metamorphic processes to which grains have been subjected while in the regolith can be clearly deduced from HVEM studies. It has been established by laboratory vacuum-annealing experiments that latent tracks and amorphous coatings, both natural and artificially produced, fade and are gradually transformed into microcrystallites of a new phase which grow as a function of temperature (17, 32). Shock deformation can fragment tracks into very short segments (55) or erase them entirely (56). We have thus been able to use latent track "metamorphism" to infer the thermal and shock history of the

constituent grains during breccia formation.

Lunar breccias can be classified on a track "micrometamorphic" scale, which provides fine distinctions at the lower end of the metamorphic sequence of six petrographic types devised by Warner (57) from optical microscopy. The least metamorphosed breccias (corresponding to types 1 and 2) contain grains with high track densities and amorphous coatings. To subdivide them according to the peak temperature reached we utilize the fact that Fe tracks fade to the extent that they become unetchable if heated a few hours at $\sim 300^\circ\text{C}$ in glass, $\sim 400^\circ\text{C}$ in olivine, and $\sim 700^\circ\text{C}$ in calcic plagioclase (27). Even though unetchable, tracks are faintly visible in plagioclase by HVEM (if stabilized by ion-thinning) (58) unless they are heated above a critical temperature at which they transform into microcrystallites. The transformation occurs at $\sim 800^\circ\text{C}$ in feldspar and $\sim 650^\circ\text{C}$ in olivine (14). Faintly visible tracks and microcrystallites correspond to subdivisions of type 3.

Gas-rich meteorites belong to a different track metamorphic type in which the tracks have not been stabilized against ionization erasure. The concentration of solar wind gas is lower than in lunar breccias and no amorphous coatings have been seen, and yet the track density is very high. In grains prepared for microscopy by crushing rather than by an ion beam, the presence of tracks can only be inferred by annealing at 800°C and then observing that microcrystallites have formed. This relative lack of maturity of the irradiated grains in gas-rich meteorites contrasts with the greater extent of microfracturing and with the stronger cementing of the grains than in lunar breccias (17).

The first observations of track-rich grains in gas-rich meteorites were made mainly by optical microscopy (59). Recently, important clues to the origin of these meteorites have emerged from electron microscopic studies of latent tracks in ion-thinned sections (33) and of replicas of lightly etched tracks in polished sections (27, 42, 60). Fayetteville and Pesyanoe, two meteoritic breccias with especially high concentrations of solar wind gases, contain a large proportion of grains with latent track densities up to 10^{11} cm^{-2} (see Fig. 9). The tracks do not cross from one grain to the next but go right up to the edges, which indicates that some of the grains were heavily irradiated and then

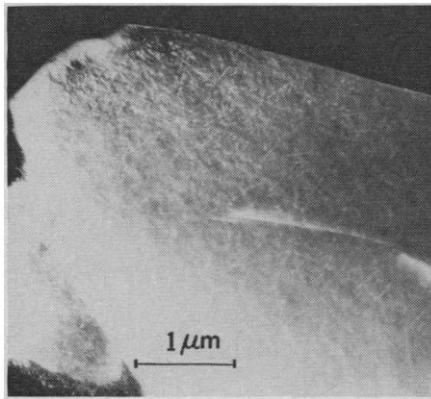


Fig. 9. High density of solar flare tracks in an ion-thinned grain from the deep interior of the Fayetteville gas-rich meteorite. This grain was irradiated on the regolith of a parent body before the meteorite was assembled.

all were compacted together so gently that no thermal or shock erasure of tracks occurred.

Studies of lightly etched replicas by TEM provide several additional clues (60). (i) More than half of the track-rich grains have been anisotropically irradiated, which indicates that they were probably exposed while on the regolith of a parent body rather than while freely orbiting the sun. (ii) The degree of anisotropy at the edges of grains (the ratio of the maximum to the minimum track density along an edge) is smaller for meteoritic breccias than for lunar breccias, which indicates that there was a more efficient stirring of the regolith of the mete-

oritic parent body than of the lunar regolith. More efficient stirring may imply that the gravitational field on the parent body was weaker than that on the moon. (iii) Both matrix grains and chondrules are track-rich. Figure 10a shows a chondrule that was broken in a collision and then irradiated anisotropically for $\sim 10^4$ years (60) before being compacted into the Fayetteville meteorite. (iv) In Kapoeta, a gas-rich meteorite with a smaller fraction (8 percent) of highly irradiated grains than Fayetteville (30 percent), some grains (Fig. 10b) preserve the record of a shock event that occurred after their irradiation, possibly during compaction of the meteorite. Tracks in these grains were partly erased by shock, and tracks may have been completely erased in other grains. Meteoritic breccias thus seem to have been produced with a wide range of shock strengths, presumably dependent on the distance of their components from the point of impact of the body responsible for their compaction. (v) Several gas-rich meteorites (Kapoeta, Bununu, and Malvern) contain small, spheroidal objects similar to the glass spheres found in all lunar soils but not nearly as common (61). Their shapes indicate that they were once molten, rotating bodies. Both lunar and meteoritic spherules contain high densities of solar flare tracks and some of them have surfaces pocked with micrometeorite craters. In both types of objects the distribution of crater diameters and the track density gradients, as well as the

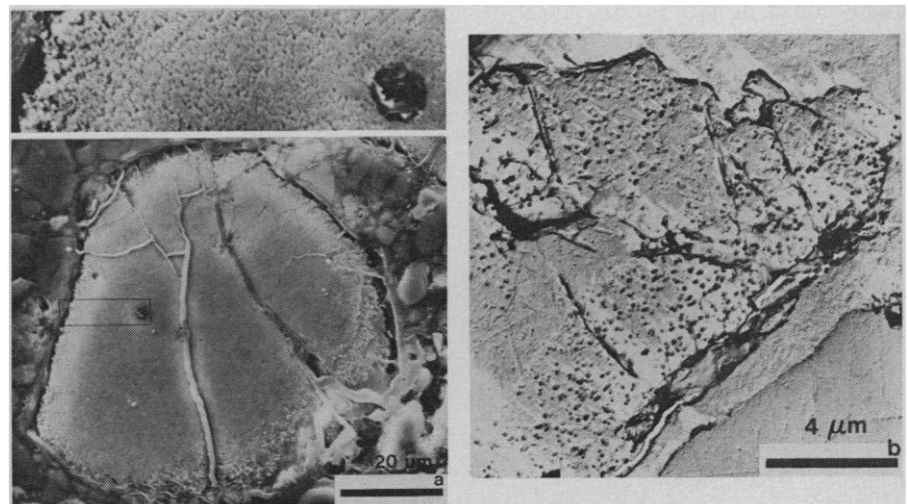


Fig. 10. Solar flare-irradiated grains in gas-rich meteorites. (a) Scanning electron micrograph of an originally spherical olivine chondrule which was broken and then irradiated anisotropically for $\sim 10^4$ years before being compacted into the Fayetteville meteorite. Tracks can be seen as a high density of pits in the portion of the etched grain in the inset; track density is highest around the rims. (b) Transmission electron micrograph of a shadowed carbon replica of an etched feldspar grain from the Kapoeta meteorite. Tracks appear as black, projecting objects with white shadows. Tracks in a strip through the grain (arrow) were erased by shock during compaction.

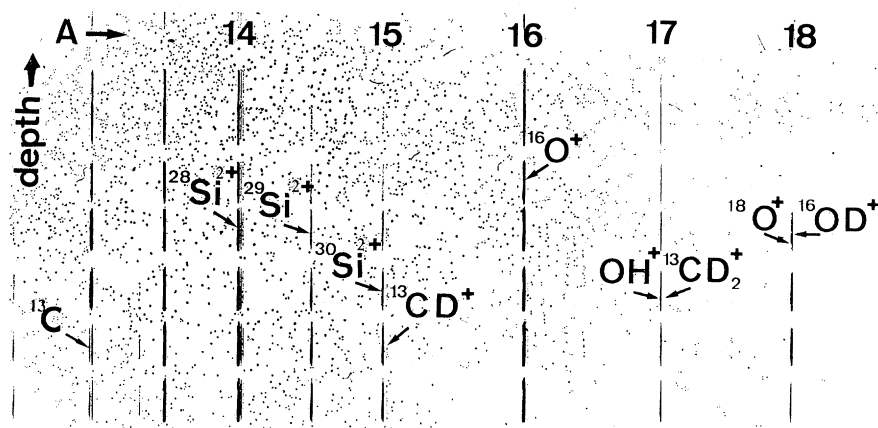


Fig. 11. Ionic analyzer study of a feldspar that was irradiated with a mixture of ^{13}C and D ions. Successive layers, each with a thickness of 100 Å, were sputtered away, and the masses of the species were analyzed as a function of depth; $A = \text{mass/charge}$. On the fourth run the ^{13}C line, as well as those corresponding to synthesized species such as ^{13}CD and OD , have disappeared as the last of the 400 Å amorphous coating has been eroded away. [Courtesy of E. Gammal and B. Vidal]

ratio of crater density to track density, are similar. This suggests that the relative fluxes of micrometeorites and of solar flare particles were rather similar during the short residence time ($< 10^6$ years) of the meteoritic and lunar dust grains on the surfaces of their parent regoliths at very different times in the past (3.7×10^9 years ago for Kapoeta and 0.5×10^9 to 1×10^9 years ago for the Apollo 15 lunar soil grains).

Solar Nebulas

Two distinct models of the formation of the solar system, both involving the process of sticking of grains, are currently under debate. In one model the accretion of interstellar dust grains into solid bodies takes place before the formation of the central star (62); in the other such an accretion can only be triggered when a young T Tauri type of star is formed (63). In both models one of the most mysterious processes is the sticking of the dust grains into giant, snowball-sized objects that can be subsequently accreted into larger bodies by gravitational forces.

The following scenario (4, 6, 64) for the sticking of dust particles in the solar nebula has attractive features, although of course it need not be a unique explanation. The turbulent dust clouds in the nebula contain a high proportion of dielectric grains that have been both rounded and coated during exposures to low-energy nuclear particles. The energy stored as radiation damage in the amorphous coatings could be released during a low-speed collision between

two grains. This could in turn "melt" the interface and make the grains stick. The plausibility of such a process is supported by studies of micrometer-sized aggregates of welded dust grains in the lunar regolith (4). Dust aggregates may have formed in this way in the early solar nebula, which very likely contained all the necessary sticking ingredients. Astronomical observations reveal the presence of dielectric grains in different types of cosmic dust clouds. Furthermore, turbulent motion of dust is predicted by all of the theories so far proposed to explain the formation of the solar system, and the collisional speed of the grains is estimated to be about 100 m/sec in the turbulent zones (62). The coatings could have been formed either in the early, superluminous phase of evolution of a star or during one of the various implantation episodes that we suggest below.

Interstellar Clouds

We mentioned earlier that the implantation of low-energy C, N, and H nuclei in dielectric solids results in the synthesis of small molecules, which are trapped in the amorphous coatings of radiation damage on the grains (4, 19, 20). The possibility that a similar process may be responsible for the formation of some of the small molecules found in interstellar clouds is discussed in detail elsewhere (4). Whatever their origin may be, the constituent dust grains of interstellar clouds have likely been exposed to very high doses of low-energy ions that could have originated in several ways: (i) in stellar winds, if

the grains were formed in a stellar atmosphere or in stellar eruptions (65); (ii) in supernova envelopes in which the grains were exposed (66); (iii) in shock waves triggered during cloud collisions (67); (iv) in the deceleration of clouds as they penetrated a galactic arm at speeds of ~ 200 km/sec, if the model of galactic arm evolution proposed by Lin (68) is right; or (v) in turbulent motion of massive molecular clouds during gravitational instabilities (69). It is tempting to postulate that small molecules could be synthesized as follows: The grains are first implanted with saturation doses of H, C, and N ions; then as soon as they are shielded from ionizing radiation, small molecules are synthesized within the ultrathin amorphous coatings; finally, during a subsequent implantation episode, the species synthesized by ion implantation are released into space by ion sputtering (Fig. 11).

The mixture of molecules found in interstellar clouds requires a highly specific synthesis, which is similar to ion implantation synthesis in that carbon compounds contain only up to three carbon atoms; OH, CH, CNH, and NH are very abundant; and very low upper limits for the concentration of NO are observed. Neither catalytic reactions of the Fischer-Tropsch type (21), nor ion-molecule reactions in the gas phase (22), nor reactions of gas adsorbed on grain surfaces (22) give rise to the right mix of molecules. We believe that ion implantation synthesis may contribute significantly to the production of the small molecules in interstellar clouds.

References and Notes

1. P. B. Price and R. M. Walker, *Nature (Lond.)* **196**, 732 (1962).
2. J. Geiss, *Proceedings of the 13th International Cosmic Ray Conference* (University of Denver, Denver, Colo., 1973), vol. 5, p. 3375.
3. J. P. Bibring, J. P. Duraud, L. Durrieu, C. Jouret, M. Maurette, R. Meunier, *Science* **175**, 753 (1972).
4. J. P. Bibring, Y. Langevin, M. Maurette, R. Meunier, B. Jouffrey, C. Jouret, P. Wszolek, *Earth Planet. Sci. Lett.*, in press.
5. J. C. Dran, L. Durrieu, C. Jouret, M. Maurette, *ibid.* **9**, 391 (1970).
6. J. Borg, M. Maurette, L. Durrieu, C. Jouret, in *Proceedings of the Second Lunar Science Conference* (MIT Press, Cambridge, Mass., 1972), vol. 3, p. 2027.
7. J. C. Dran, M. Maurette, M. Dumail, J. P. Duraud, *Meteoritics* **8**, 347 (1973).
8. J. P. Bibring, M. Maurette, R. Meunier, L. Durrieu, C. Jouret, O. Eugster, in *Lunar Science III* (Lunar Science Institute, Houston, Tex., 1972), p. 71.
9. J. Borg, private communication.
10. J. P. Bibring, J. Chaumont, G. Comstock, M. Maurette, R. Meunier, R. Hernandez, in *Lunar Science IV* (Lunar Science Institute, Houston, Tex., 1973), p. 72.
11. L. A. Fisk, private communication.
12. G. K. Wehner, C. E. Kenknight, D. L. Rosenberg, *Planet. Space Sci.* **11**, 1257 (1963).
13. J. A. M. McDonnell and R. P. Flavill, in *Lunar Science V* (Lunar Science Institute, Houston, Tex., 1974), p. 478.

14. J. P. Bibring, thesis, Faculté des Sciences d'Orsay (1972).
15. For a review, see F. Hörz, D. E. Brownlee, H. Fechtig, J. B. Hartung, D. A. Morrison, G. Neukum, E. Schneider, J. F. Vedder, *Planet. Space Sci.*, in press.
16. J. Borg, G. M. Comstock, Y. Langevin, M. Maurette, C. Thibaut, in *Lunar Science V* (Lunar Science Institute, Houston, Tex., 1974), p. 79.
17. J. C. Dran, J. P. Duraud, M. Maurette, L. Durrieu, C. Jouret, C. Legressus, in *Proceedings of the Third Lunar Science Conference* (MIT Press, Cambridge, Mass., 1972), vol. 3, p. 2883.
18. D. Heymann and A. Yaniv, in *Proceedings of the Apollo Lunar Science Conference* (Pergamon, New York, 1970), vol. 2, p. 1261.
19. This hypothesis is supported by a study of the thermal release of ^{13}C species in silicate targets that were bombarded with high doses of low-energy ^{13}C ions. See J. P. Bibring, A. Burlingame, J. Chaumont, Y. Langevin, M. Maurette, P. Wszolek, in *Proceedings of the Fifth Lunar Science Conference* (MIT Press, Cambridge, Mass., in press).
20. J. P. Bibring, A. Burlingame, J. Chaumont, M. Maurette, G. Slodzian, P. Wszolek, in *Lunar Science V* (Lunar Science Institute, Houston, Tex., 1974), p. 57.
21. E. Anders, *Science* **182**, 781 (1973).
22. W. D. Metz, *ibid.*, p. 466.
23. J. P. Bibring, A. L. Burlingame, J. P. Duraud, M. Maurette, J. T. O'Connor, F. C. Walls, P. Wszolek, in *Proceedings of the Fifth Lunar Science Conference* (MIT Press, Cambridge, Mass., in press).
24. Total carbon was measured by P. H. Cadoogan, G. Eglinton, J. N. M. Firth, J. R. Maxwell, B. J. Mays, C. T. Pillinger [in *Proceedings of the Third Lunar Science Conference* (MIT Press, Cambridge, Mass., 1972), vol. 2, p. 2069].
25. Albedos were measured by A. Dollfus.
26. D. J. Barber and P. B. Price, in *Proceedings of the 25th Anniversary Meeting of the Electron Microscopy Association of Great Britain* (Institute of Physics, London, 1971).
27. D. Macdougall, R. S. Rajan, I. D. Hutcheon, P. B. Price, in *Proceedings of the Fourth Lunar Science Conference* (Pergamon, New York, 1973), vol. 3, p. 2319.
28. W. H. Huang and R. M. Walker, *Science* **155**, 1103 (1967).
29. J. Borg, M. Maurette, R. M. Walker, E. Zimmer, in *Lunar Science V* (Lunar Science Institute, Houston, Tex., 1974), p. 76.
30. E. C. H. Silk and R. S. Barnes, *Phil. Mag.* **4**, 970 (1959).
31. J. Borg, J. C. Dran, L. Durrieu, C. Jouret, M. Maurette, *Earth Planet. Sci. Lett.* **8**, 379 (1970).
32. L. Durrieu, C. Jouret, C. Lerouley, M. Maurette, *Jernkontorets Ann.* **155**, 535 (1971).
33. D. J. Barber, R. Cowsik, I. D. Hutcheon, P. B. Price, R. S. Rajan, in *Proceedings of the Second Lunar Science Conference* (MIT Press, Cambridge, Mass., 1971), vol. 3, p. 2705.
34. P. B. Price, D. Lal, A. S. Tamhane, V. P. Pereygin, *Earth Planet. Sci. Lett.* **19**, 377 (1973).
35. G. Bastin, G. M. Comstock, J. C. Dran, J. P. Duraud, M. Maurette, C. Thibaut, in *Lunar Science V* (Lunar Science Institute, Houston, Tex., 1974), p. 44.
36. E. Dartige, unpublished results.
37. I. D. Hutcheon, D. Macdougall, P. B. Price, in *Proceedings of the Fifth Lunar Science Conference* (MIT Press, Cambridge, Mass., in press).
38. D. J. Barber, I. Hutcheon, P. B. Price, *Science* **171**, 372 (1971).
39. J. Borg, M. Maurette, L. Durrieu, C. Jouret, J. Lacaze, P. Peters, in *Lunar Science III* (Lunar Science Institute, Houston, Tex., 1972), p. 92.
40. Quantitative evidence for the flattening of track gradients by erosion of lunar rocks is summarized in G. Crozaz, R. Drozd, C. M. Hohenberg, H. P. Hoyt, D. Ragan, R. M. Walker, D. Yuhas, in *Proceedings of the Third Lunar Science Conference* (MIT Press, Cambridge, Mass., 1972), vol. 3, p. 2917.
41. P. B. Price, J. H. Chan, I. D. Hutcheon, D. Macdougall, R. S. Rajan, E. K. Shirk, J. D. Sullivan, in *Proceedings of the Fourth Lunar Science Conference* (Pergamon, New York, 1973), vol. 3, p. 2347.
42. R. S. Rajan, *Geochim. Cosmochim. Acta* **38**, 777 (1974).
43. J. Borg, unpublished results.
44. I. D. Hutcheon, D. Braddy, P. P. Phakey, P. B. Price, in *Apollo 15 Sample Studies* (Lunar Science Institute, Houston, Tex., 1972), p. 412.
45. I. D. Hutcheon, D. Macdougall, P. B. Price, in *Lunar Science V* (Lunar Science Institute, Houston, Tex., 1974), p. 378.
46. Large-scale erosion resulting from micro-meteorite collisions is quite discontinuous, and as long as the track-recording surface has been exposed for less than $\sim 10^9$ years, it is possible to measure track density as a function of depth on a crystal that is free of craters. Continuous erosion from solar wind sputtering can be avoided if the track-recording surface is shielded from direct view of the sun but is still exposed to space. For example, a crystal at the bottom of a vug or cavity in a rock that "looks" only perpendicular to the ecliptic plane will not be eroded by the solar wind but can collect tracks from solar flare ions, whose angular distribution is made nearly isotropic by scattering from magnetic field irregularities (44).
47. D. A. Papanastassiou, R. S. Rajan, J. C. Huneke, G. J. Wasserburg, in *Lunar Science V* (Lunar Science Institute, Houston, Tex., 1974), p. 583.
48. D. Macdougall and P. B. Price, *Meteoritics*, in press.
49. G. Crozaz and R. M. Walker, *Science* **171**, 1237 (1971); R. L. Fleischer, H. R. Hart, G. M. Comstock, *ibid.*, p. 1240.
50. P. B. Price, I. Hutcheon, R. Cowsik, D. J. Barber, *Phys. Rev. Lett.* **26**, 916 (1971).
51. R. L. Fleischer and H. R. Hart, *ibid.* **30**, 31 (1973); D. Braddy, J. Chan, P. B. Price, *ibid.*, p. 669; D. Burnett, C. Hohenberg, M. Maurette, M. Monnin, R. Walker, D. Wollum, in *Apollo 16 Preliminary Science Report* (NASA SP 315, National Aeronautics and Space Administration, Washington, D.C., 1972), chap. 15, p. 19.
52. L. A. Frank, *J. Geophys. Res.* **75**, 707 (1970).
53. R. P. Lin, C.-I. Meng, K. A. Anderson, *ibid.* **79**, 489 (1974).
54. E. M. Shoemaker, M. H. Hait, G. A. Swann, D. L. Schleicher, G. G. Schaber, R. L. Sutton, D. H. Dahlem, E. N. Goddard, A. C. Waters, *Geochim. Cosmochim. Acta* **3** (Suppl. 1), 2399 (1970).
55. R. L. Fleischer, G. M. Comstock, H. R. Hart, *J. Geophys. Res.* **77**, 5050 (1972).
56. R. L. Fleischer, R. T. Woods, H. R. Hart, P. B. Price, *ibid.* **79**, 339 (1974).
57. J. L. Warner, in *Lunar Science III* (Lunar Science Institute, Houston, Tex., 1972), p. 782.
58. I. D. Hutcheon, P. P. Phakey, P. B. Price, in *Proceedings of the Third Lunar Science Conference* (MIT Press, Cambridge, Mass., 1972), vol. 3, p. 2845; P. P. Phakey, I. D. Hutcheon, R. S. Rajan, P. B. Price, in *ibid.*, vol. 3, p. 2905.
59. D. Lal and R. S. Rajan, *Nature (Lond.)* **223**, 269 (1969); P. Pellas, G. Poupeau, J. C. Lorin, H. Reeves, J. Audouze, *ibid.*, p. 272.
60. D. Macdougall, R. S. Rajan, P. B. Price, *Science* **183**, 73 (1974).
61. D. E. Brownlee and R. S. Rajan, *ibid.* **182**, 1341 (1973); R. S. Rajan, D. E. Brownlee, F. Hörz, in *Lunar Science V* (Lunar Science Institute, Houston, Tex., 1974), p. 616.
62. A. G. W. Cameron, in *Origin of the Solar System*, H. Reeves, Ed. (CNRS, Paris, 1972), p. 56.
63. V. S. Safranov, in *ibid.*, p. 89.
64. J. P. Bibring and M. Maurette, in *ibid.*, p. 156.
65. H. Spinrad and R. F. Wing, *Annu. Rev. Astron. Astrophys.* **7**, 249 (1969).
66. J. Borg, J. C. Dran, G. Comstock, J. P. Duraud, M. Maurette, B. Vassent, in *Lunar Science IV* (Lunar Science Institute, Houston, Tex., 1973), p. 82.
67. P. A. Aannestad, *Astrophys. J. Suppl.* **25**, 223 (1973).
68. C. C. Lin, *Highlights Astron.* **2**, 88 (1971).
69. D. M. Rank, C. H. Townes, W. J. Welch, *Science* **174**, 1083 (1971).
70. M.M. thanks R. Klapisch and B. Joffrey for their enthusiastic support and interest and C. Jouret for his superb assistance during the HVEM observations. The research of P.B.P. was supported by the Lunar Programs Office, National Aeronautics and Space Administration.